Academic Education Publishing House
Industry Science and Engineering Vol. 1 No. 9, 2024

Simulation and Optimization of Sand Mixing Device

Shimao Zhang[1,2], Hao Zhou[1,2], Qi Xia[2], Minwei Qiu[1], Manlai Zhang[1,2,*], Zhiqiang Zhang[1,*]
[1]*School of Mechanical Engineering, Yangtze University, Jingzhou, Hubei, China*
[2]*Key Laboratory of Oil and Gas Production, Yangtze University, China National Petroleum Corporation, Jingzhou, Hubei, China*
**Corresponding Author.*

Abstract: **In response to the requirements for rapid mixing and erosion resistance of sand mixing devices used in hydraulic fracturing at high flow rates, computational fluid dynamics methods and discrete multiphase flow models were used to conduct three-dimensional unsteady simulations of the internal flow field of commonly used typical sand mixing devices. The mixing efficiency and sand particle motion trajectory were obtained, and the erosion wear on the inner wall of the sand mixing device was obtained through the DPM erosion model. On this basis, the influence of blade quantity, length, and angle on the erosion and wear life of the device is explored. The research results indicate that the optimal combination of 4 long and 4 short blades with an inclination angle of 60 ° increases the erosion life by 54% with an increase in the number of blades and the structure of the long and short blades. At this point, the lifespan of the impeller mixed with sand is 401 hours.**

Keywords: Sand Mixing Devices; Mixing Efficiency; DPM Erosion Model; Wear Life of the Device; Lifespan of the Impeller

1. Introduction

Hydraulic fracturing is one of the main technical means to realize the commercial development of low-permeability and ultra-low-permeability oil and gas fields such as shale gas in China. By injecting fracturing fluid downhole, fracturing the reservoir and communicating with natural fractures to form a network of seams, the porosity of the reservoir can be greatly increased, and ultimately, the production of a single well can be increased [1-3].Currently, hydraulic fracturing technology is developing in the direction of high flow rate and high pressure, which puts higher requirements on the sand mixing equipment for preparing fracturing fluids, and the mixing performance and erosion and abrasion resistance of the equipment under high flow rate need to be improved in order to meet the requirements of the fracturing process parameters and continuous and stable operation [4-6]. Raghav and Joshi [7] investigated the off-bottom clearance of the straight (slanting) paddles, and found that off-bottom spacing is positively correlated with the mixing time. Fan et al. [8] found the relationship between liquid flow characteristics and particle motion characteristics. Xu and Zhao [9] found that the installation height of the impeller is too high or too low will reduce the mixing efficiency. Wan et al. [10] found that the higher the rotational speed of the impeller, the higher the mixing quality. However, the power of the mixing tank will rise rapidly with it. Huang et al. [11] found that the diameter of the upper impeller had the greatest influence on the mixing efficiency, and the ratio of the upper impeller guide cylinder to the impeller diameter had the least influence on the mixing efficiency. Xu et al. [12] concluded that the Multi-blade combined mixing paddles are more effective than the commercial Max blend mixing paddles in mixing high viscosity fluids. And the turbulent energy is more evenly distributed, allowing the particles to be dispersed into the base fluid faster. Wang et al. [13] obtained the motion characteristics of solid particles in the impeller. Qian et al. [14] obtained the flow characteristics of two-phase flow of water and sand in a centrifugal pump. Wu et al. [15] established the relationship between impeller speed, vane parameters and particle size in the flow channel of slurry pump.

At present, the common optimization methods of sand blending device are mainly aimed at improving the efficiency of sand blending device, but less for the optimization of device life. In this paper, CFD and DPM models are used to simulate the flow characteristics of liquid and solid two-phase flow and the erosion wear characteristics of the overflow parts, and further optimize the structure of the sand mixing equipment. To obtain the optimal Impeller blade deflection angle, number of blades, length and length of blade structure, calculation of corrosion and wear life, for mixing will have a certain guiding role and discharge tank in practical applications, and improve the service life of sand mixing equipment.

2. Structure and Working Principle of Sand Mixing Device

The general structure of the sand mixing device used in this paper is shown in Figure 1 and the cylinder with a plate thickness of 15mm and a diameter of 960mm and a height of 620mm is used as the main cavity of the mixing and discharging tank. The inlet and outlet of the mixing tank are tangent to the tank body, the diameter of the inlet is 200mm, and the diameter of the outlet is 260mm. Clean water is introduced into the device through the suction inlet suction pipe. Clean water are rapidly mixed through the high-speed rotating impeller, and finally discharged from the discharge pipe mouth. The whole sand mixing process is only carried out inside the device, ignoring the influence of the sand bucket structure on the sand mixing process, and only the impeller is modeled. When the solid particles are in contact with the blade, the blade accelerates to make circular motion, and the particles slide on the blade surface, causing scratches on the blade surface. When a large number of solid particles pass through the blade, the blade wear becomes serious.

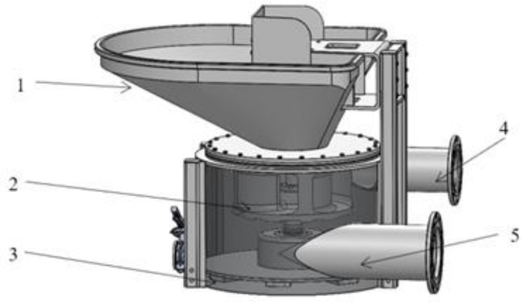

1 Sand hopper; 2 Impeller; 3 Tank; 4 Suction nozzle; 5 Discharge port

Figure 1. Model of Sand Mixing Device

In the sand mixing equipment, the most important component is the impeller, and the good or bad design of the impeller directly affects the performance of the whole sand mixing device. The structure of the impeller is shown in Figure 2, which can be divided into one main impeller and two upper and lower secondary impellers. The upper vice impeller is used for sealing, and the lower vice impeller is used for stirring the mixing liquid.

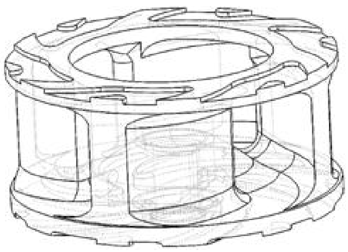

a. Impeller Body

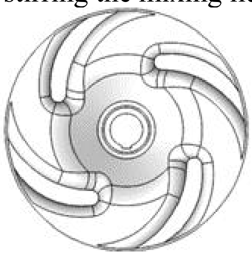

b. Impeller Main Impeller (Truncated)

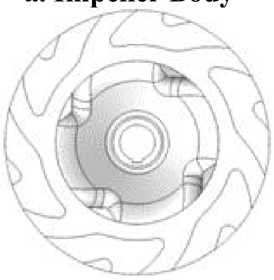

c. Upper Secondary Impeller

d. Lower Impeller

Figure 2. Impeller Structure

2.1 Calculation Method and Simulation Modeling

The mixing motion of solid particles and water belongs to solid-liquid two-phase flow, which needs to be described by the introduction of a multiphase flow model. Commonly used multiphase flow models for CFD are VOF, Mixture and Eulerian [16]. In this paper, the simulation of the internal flow field is calculated by using the Mixture model.

Continuity equation [17]:

$$\frac{\partial}{\partial t}(\rho_m) + \nabla \cdot (\rho_m \vec{v}_m) = 0 \tag{1}$$

Momentum equation:

$$\frac{\partial}{\partial t}(\rho_m \vec{v}_m) + \nabla \cdot (\rho_m \vec{v}_m \vec{v}_m) = -\nabla p + \nabla \cdot [\mu_m(\nabla \vec{v}_m + \vec{v}_m^T)] + \rho_m \vec{g} + \vec{F} + \nabla \cdot (\sum_{k=1}^{n} \alpha_k \rho_k \vec{v}_{dr,k} \vec{v}_{dr,k}) \tag{2}$$

Where.$\vec{v}_m$ is the mass average velocity;ρ_m is the mixed density; n is the number of phases; $\vec{F}$ is the volume force; μ_m is the mixing viscosity;$\vec{v}_{dr,k}$ is the drift velocity of the second phase k$\vec{v}_{dr,k} = \vec{v}_k - \vec{v}_m$;p is the pressure on the impeller shaft; g is the gravitational acceleration;ρ_k is the density of the kth phase; α_k is the volume fraction of phase k;

The erosion of the flow channel by solid particles is calculated using DPM model [18]. Water is used as the medium, the impeller speed is 1200 rpm, and the particle phase enters the flow field by incidence. Smooth sphere is selected for particle properties. The number of iteration steps for the continuous phase is set to 10. The maximum value for calculating individual orbital time steps is set to 500. the physical model in the DPM model option is set to wear/deposition and two-phase turbulent coupling. Set the inlet and outlet discrete phase walls to "Escape" and set the rest of the discrete phase walls to "Reflection". The Reynolds vortex-viscosity model is used to solve the continuous phase flow control equation, and the Reynolds-averaged derivation of the three-dimensional steady state N-S equation is processed. Assuming that in the stirred flow field, the discrete phase and the continuous phase motion process do not affect each other, then the motion law of the continuous phase is in accordance with the conservation of mass, and the continuity equation of the liquid-phase flow in the stirred flow field can be obtained as follows:

$$\frac{\partial \rho_f}{\partial t} + \frac{\partial(\rho_f u_j)}{\partial x_j} = 0 \tag{3}$$

Since the multiphase flow in the stirred flow field is an incompressible fluid and ρ is a constant, the liquid-phase flow in the stirred flow field. The momentum equation for the:

$$\frac{\partial}{\partial t}(\rho_f u_i) + \frac{\partial}{\partial x_j}(\rho_f u_i u_j) = -\frac{\partial p}{\partial x_i} + \frac{\partial}{\partial x_j}[\mu_e\left(\frac{\partial u_j}{\partial x_i} + \frac{\partial u_i}{\partial x_j}\right)] - 2\rho_f e_{ilk}\omega_{luk} + \frac{\rho_s}{\tau_{rs}}(u_{s_i} - u_i) \tag{4}$$

In the formula: ρ_f denotes the density of the liquid phase; t denotes time; u velocity vector; s, f denote the solid phase and liquid phase, respectively; τ_{rs} The relaxation time of the solid phase particle motion process; P the equivalent pressure of the centrifugal force; μ_e Equivalent viscous coefficient.

2.2 CFD Simulation

2.2.1 Geometric modeling 3D drawing

Space Claim software performs structural meshing of the model. Mesh encryption was performed in the high gradient region with the motion region as shown in Figure 3a, with mesh encryption in the high gradient region with the motion region. Two cross-sections are established on the flow channel model of the mixing device, and the blades are divided into A and B planes, with a total of 4 blades. As shown in Figure 3a, cross-section 1 coincides with the YZ plane, cross-section 2 is parallel to the ZX plane, the center region of the impeller on cross-section 2 is delineated as a square region of 0.1m*0.1m, and the pressure value of the center of the impeller is taken as the average of the pressure in the region.

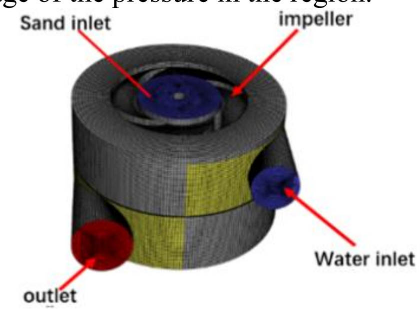

a. Flow Channel Grid Model of Sand Mixing Device

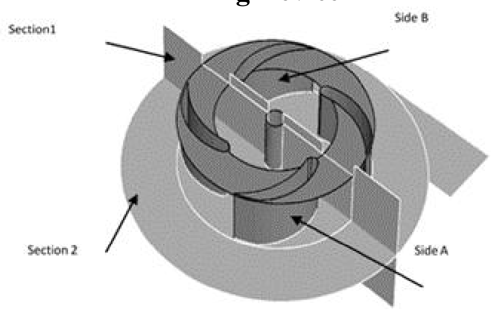

b. Schematic of Cross-Section Distribution

Figure 3. Sand Mixing Device Model

Table 1 shows the grid independence analysis table. When the number of grid division is 980,000, continue to increase the number of grids, the difference between the parameters is small, the grid is considered to meet the independence requirements, and the final number of grids is determined as 980000.

Table 1. Grid Independence Analysis Table

Mesh Type	Grid 1	Grid 2	Grid 3	Grid 4	Grid 5
Number of grids	682,00	784,000	980,000	1,059 million	1.125 million
Maximum erosion rate (kg-6/m^2)	0.81	0.94	1.1	1.11	1.13

2.2.2 CFD boundary conditions

The pressure and velocity fields are analyzed and calculated using the SIMPLE algorithm, and the discrete format gradient is obtained using the Least Squares Cell Based method. The first order upwind format is used for both turbulent kinetic energy and turbulent energy dissipation rate terms. The accuracy of calculating residuals is set to 10-4 A transient flow field is used for simulation, and a large vortex is formed in the tank when the mixing and discharge unit is in operation. Therefore, it is necessary to use the RNG k-ε turbulence model for vortex simulation [19]. The inlet of the flow field of the mixing tank is a mass inflow port with a rate of 100 kg/s. The outlet is a pressure outlet with a pressure of 0.45 MPa. When the rotating speed of the impeller is high, negative pressure is generated in the center of the impeller, at this time, the air and solid materials enter into the mixing tank from the sand inlet. The sand inlet is set up as a pressure outlet, and the pressure is the same as atmospheric pressure. The impeller movement area is processed by the dynamic grid method, and its speed size is from 0 to 1200 r/min.

2.2.3 Analysis of simulation results

Figure 4a shows the air-liquid distribution in the impeller channel without considering particles on section 1, the impeller center vortex region only air, vortex edge of the gas-liquid two-phase was mixed, preventing the periphery of the high-pressure liquid into the center of the low-pressure region, so that the pressure of the periphery is not affected by the liquid from the center of the impeller overflow (pressure retention performance). Figure 4b shows the distribution of particles in the middle section of the impeller. The particles are gathered in the center region of the impeller, and are rapidly centrifuged to the outer region of the impeller after contacting with the blades, the particles are in contact with the A side of the blades more, and the motion speed of the particles after contacting has been significantly improved, so the rate of erosion and wear on the A side is much greater than that on the B side of the blades.

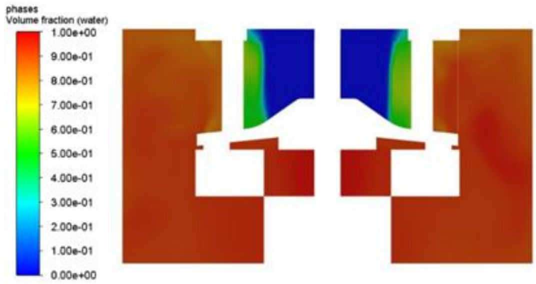

a. Schematic Diagram of Gas-Liquid Distribution

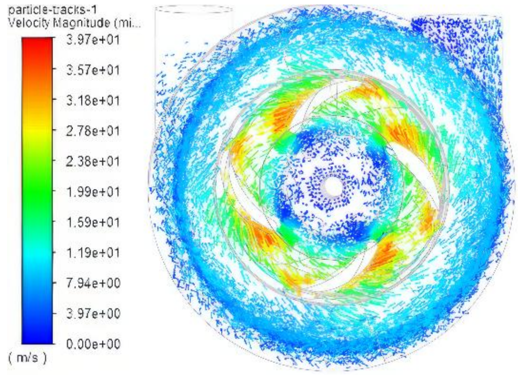

b. Schematic of Particle Velocity

Figure 4. Simulated Cloud Map

3. Structural Optimization Analysis

3.1 Simulation Analysis of Impeller with Different Deflections, Quantities and Structures

Figure 5 shows the pressure cloud on the cross-section (section 2), with the blade deflection angle of 60° as a reference, and the blade deflection angle of the control group is set to 66°, 63°, 57°, 54°. Figure 5 shows the pressure cloud map on the cross-section. Comparing the pressure cloud maps of the impellers with different deflection angles, it can be found that the maximum and minimum pressure changes on the impeller are not significant after the blade deflection angle is changed.

The number of impeller blades is 3/5/6 as a control group, and the pressure values at the center of the impeller at the same rotational speed are used to compare the performance of impellers with different numbers of blades. Figure 6 shows the pressure cloud on the cross-section, and the pressure peaks all appear on the blade A surface. With the increase of the number of blades, the area of peak pressure on the A-surface of the blade decreases gradually.

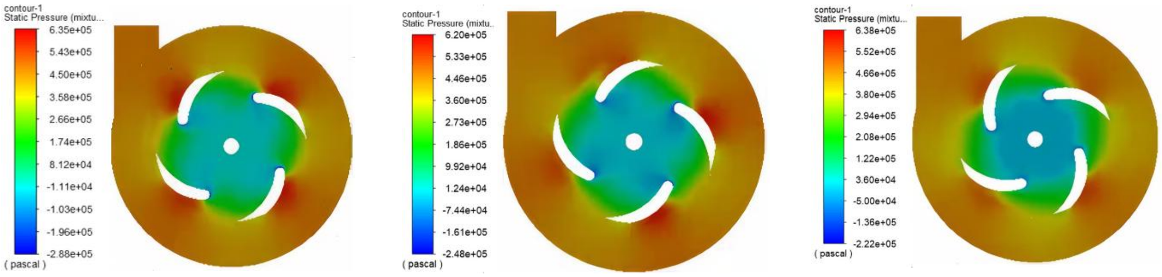

a. 54° Angle of Declination **b. 57° Angle of Declination** **c. 63° Angle of Declination**

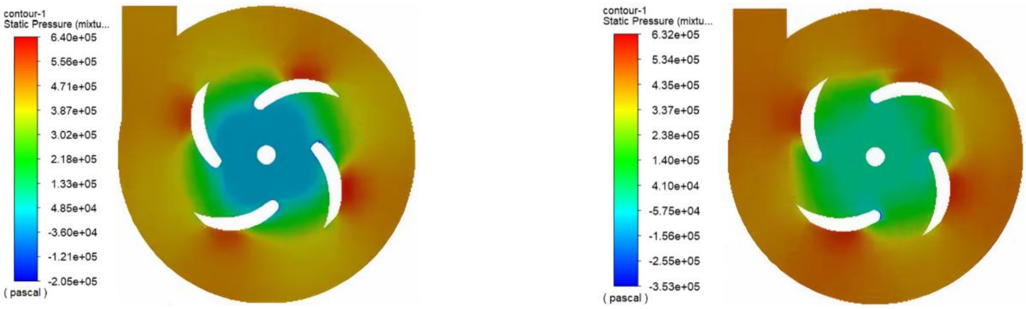

d. 66° Angle of Declination **e. 60° Angle of Declination**

Figure 5. Pressure Cloud for Different Deflection Angles

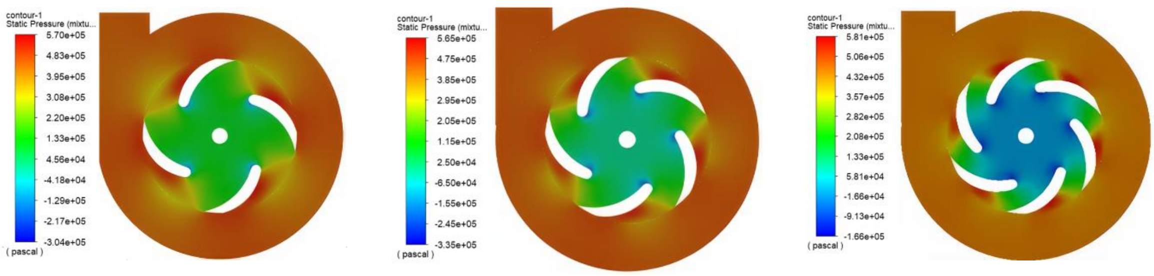

a. 4-bladed Impeller **b. 5-bladed Impeller** **c. 6-bladed Impeller**

Figure 6. Pressure Cloud for Different Number of Blades

Short blades are added to the impeller with blade number 4/5/6. Figure 7 shows the pressure cloud. Compared with the normal impeller, the peak pressure of the impeller with short blades still occurs on the A-side of the blades, but the area of the peak pressure region is smaller and is concentrated at the end of the blades.

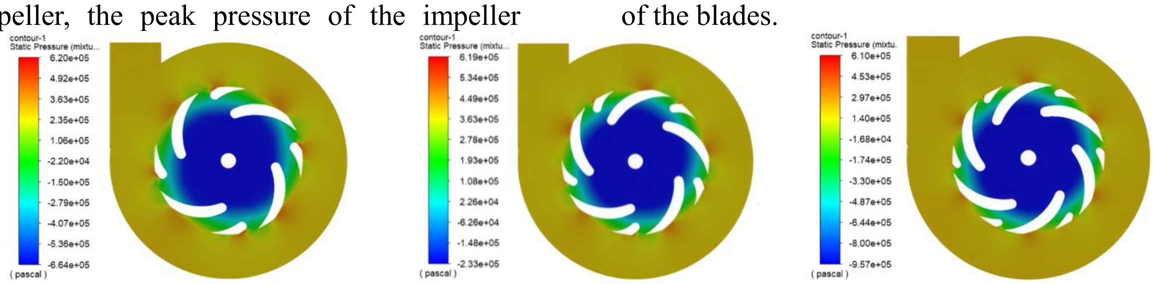

a. 4-bladed Impeller **b. 5-bladed Impeller** **c. 6-bladed Impeller**

Figure 7. Pressure Clouds for Long and Short Blades

Figure 8a shows the relationship between the pressure at the center of the impeller and the rotational speed after changing the blade deflection angle. Based on the simulation results of the impeller (original impeller) with a blade deflection angle of 0 When the blade deflection angle is 60°. increasing or decreasing the blade deflection angle, the improvement of blade performance is no longer obvious, so the blade deflection angle is already in the range of a reasonable value. Figure 8b shows the relationship between impeller center pressure and rotational speed by changing the number of impeller blades. When the number of blades is increased from 4 to 6, the pressure value of the impeller center decreases at the same rotational speed, which is conducive to the improvement of blade

Academic Education Publishing House
-AEPH-

performance. Figure 8c-e shows the comparison of impeller center pressure with different number of blades after adding short blades. The center pressure of the impeller with short blades is smaller than that of the ordinary impeller without short blades, and the addition of short blade structure can improve the pressure holding performance of the impeller.

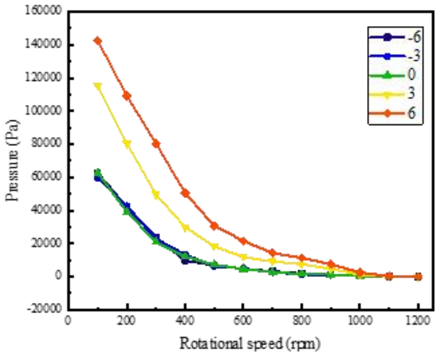

a. Different Angles

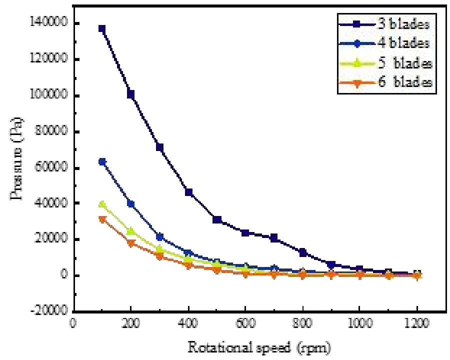

b. Varying Quantities

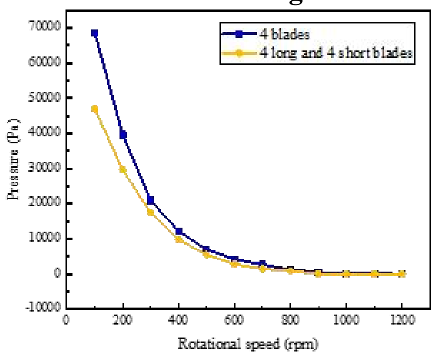

c. 4 Long and 4 Short Blade Impellers

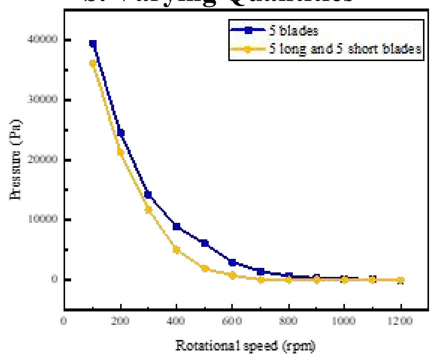

d. 5 Long and 5 Short Blade Impellers

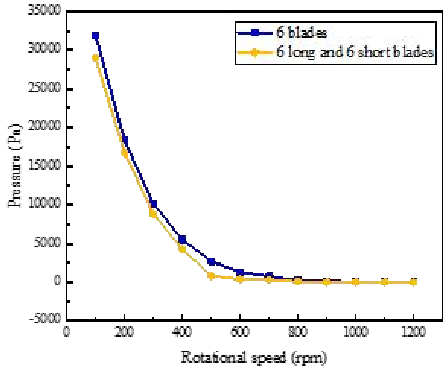

e. 6 Long and 6 Short Blade Impellers

Figure 8. Relationship between Center Pressure of Each Impeller and Impeller Speed

3.2 Analysis of Sand Mixing Performance

The performance of the mixing unit depends on the degree of mixing of the sand particles. The time for the outlet particle concentration to reach a stable value is used as the main parameter to measure the mixing performance of the impeller. The variation of export particle concentration with time is shown in Figure 9. After changing the impeller structure, the impeller channel width of the 4-blade impeller model is relatively large, and the time to reach stable concentration is also the shortest, the 6-blade length blade impeller takes the longest time to reach the stable concentration.

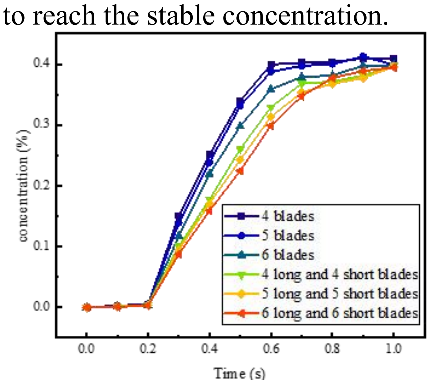

Figure 9. Relationship between Outlet Grain Concentration and Time

4. Erosion and Wear Simulation and Life Calculation

Under the condition of considering blade performance and mixing degree, the impeller with 4 blades, 4 long blades, 4 short blades and 5 blades were selected to carry out erosion wear analysis.

4.1 Numerical Simulation of Erosive Wear

Figure 10 shows the amount of wear on the impeller wall, and from the distribution location of the erosion wear, the fastest region of the impeller wear is the head of the blade near the bottom of the impeller. This is caused by the entry of particles in the discrete phase into the impeller region in the direction of the impeller axis. The movement of the particles towards the blades after contacting the impeller end face results in the concentration of the erosive wear region in the lower part of the blades.

Evaluate the improvement of erosive wear. The continuous phase inside the tank is water with a kinetic viscosity of 1.003·10-3Pa · s and a density of 998.2kg/m^3; the discrete phase is solid particles with a density of 1720 kg/m^3; and the number of incident particles in the discrete phase is 40,000, with a particle size of 0.27mm. Selecting a discrete phase erosion wear model for calculating wear amount. According to the actual sand inlet speed, the maximum erosion rates of 4 blade, 5 blade, 4 long and 4 short blade impellers are 2.05e-6kg/m^2, 1.3e-6 kg/m^2 and 1.1e-6kg/m^2, respectively.

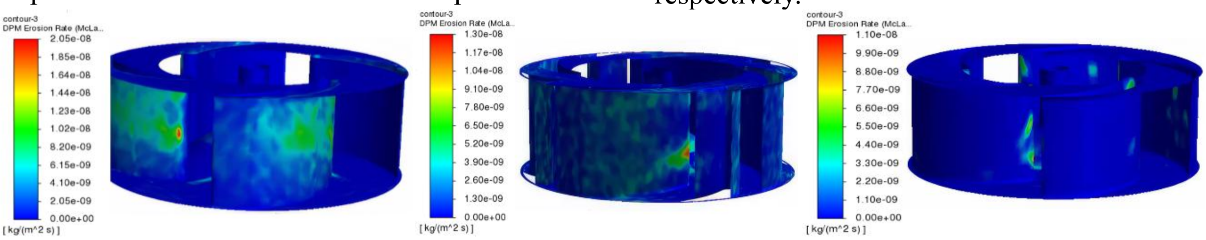

a) 4 Blade Impeller **b) 4 Long and 4 Short Blade Impellers** **c) 5 Blade Impeller**

Figure 10. Wear Amount of Impeller Wall Surface

4.2 Lifetime Estimation

The Archard Wear Model is one of the most widely used models in practice today. During the numerical simulations, the maximum flow rate of the sand mixing device is 10 m^3/min [20]The concentration of solid-phase particles in the mixing liquid is 40%, and the particle size of the actual sand particles varies, so in order to facilitate the calculation, the sand particles are unified into 50 purpose sand particles, from which the number of solid particles N in the mixed discharge tank can be obtained per unit time.

$$N = \frac{M}{\rho_{\text{sand}} V} \tag{5}$$

In the formula: M is the mass of sand particles entering the mixing tank per unit time; ρ_{sand} is the density of sand particles; V is the volume of a single sand grain.

The wear rate of the impeller is converted into the wear depth h per unit time, and the number of incident particles is controlled. This means that the erosion wear rate R_n generated by the sand mixing device after mixing n particles is determined. Subsequently, the actual erosion wear rate R_t per unit time in the mixing tank can be calculated by determining the number of particles N required for actual operation of the sand mixing device.

$$R_t = R_n \frac{N}{n} \tag{6}$$

Construct a computational model for the wear depth, h, per unit time:

$$h = \frac{R_t \Delta t}{\rho} \tag{7}$$

In the formula: ρ -density of material; Δt -unit time;

The maximum wear speed h of the 4-blade impeller and the 5-blade impeller is

$$h_4 = R_n \frac{N \Delta t}{n \rho} = 0.0015675 mm/s \tag{8}$$

$$h_5 = 0.0008414 mm/s \tag{9}$$

$$h_{4\ long\ and\ 4\ short\ blades} = 0.0007135 mm/s \tag{10}$$

The thickness of the impeller blade is 38mm, and the wear thickness under the actual working condition is half of the initial thickness, then the impeller device is judged to be failed, and at this time, the life of the 4-bladed impeller, the 5-bladed impeller, and the 4-long and 4-short impellers are 260h, 340h, and 401h respectively.

5. Conclusion

(1) Through simulation, it is found that blades with 4 long and 4 short declination angles of 60° have longer service life, and the pressure in the central region is less.
(2) With the increase of the number of blades, when the number of blades increases from 3 to 6, the central pressure of the impeller gradually decreases.
(3) By adding short blades, the pressure holding capacity of the impeller is more obviously improved, but when the number of impeller blades is high, adding short blades has a greater impact on the mixing efficiency.

Acknowledgments

This study was supported by the Educational Commission of Hubei Province of China (B2016032), and the National Natural Science Fund Project (62173049).

References

[1] DAN J. Evaluation of Hydrocarbon Generation and Storage in the Barnett Shale, Ft. Worth basin, Texas. Texas: Humble Geo-chemical Services Division, 2004.
[2] CHEN Chao, JIANG Yong, MIAO Honghai, RUAN Baosheng. Fracturing Technology and Development Trend of Low Permeability Oil Field. China Petroleum and Chemical Standard and Quality, 2019, 39(04): 247-248.
[3] LI Chaoping. Fracturing Technology and Development Trend of Low Permeability Oil Field. Petrochemical Industry Technology, 2017, 24(08): 152.
[4] LI Xinming. The Research on Liquid-Solid Two-Phase Flow and Impeller Wear Characteristics in the Slurry-Mixing Tank. Central South University, 2012.
[5] HUO Guang, QI Jian, LI Xuan, CHE Yongshun. Characteristics and Development Trend of Mixing Device in Mixed Sand Truck. Petrochemical Industry Technology, 2015, 22(09).
[6] ZHAO Jing, CHEN Xianming, GAO Zhengming. Experimental Study and Numerical Simulation of Fluid Flow in a Liquid Multiple Impeller Stirred Tank. Journal of Beijing University of Chemical Technology (Natural Science Edition), 201103017.
[7] RAGHAV R, JOSHI J Liquid phase mixing in mechanically agitated vessels. ChemEngCommun,1988,74(1):1-25.
[8] FAN L, MAO Z, WANG Y. Numerical simulation of turbulent solid-liquid two phase flow and orientation of slender particles in a stirred tank. Chemical Engineering Science, 2005, 60: 7045-7056.
[9] XU Zhuo, ZHAO Hengwen. Numerical Simulation on the Mixing Effect of OAR Type Stirrer Installation Height. Machine Building& Automation, 2013, 41(2): 178-181.
[10]WAN Zhenzhou, HUA Jian, YIN Zhen, ZHAO Fei, ZHENG Zhun. Numerical Simulation of the Flow Field and Power of the Blender Mixing Tank. China Petroleum Machinery, 2014, 42(2): 80-83.
[11]HUANG Tiancheng, ZHOU Sizhu, YUAN Xinmei, WANG Deguo. Structural Optimization of Mixing Impellers in Fracturing Sand Mixing Device. Journal of Southwest Petroleum University (Science Technology Edition), 2019, 41(04): 159-165.
[12]XU Yan,WANG Jian, WU Yongjun, LUO Peicheng. Study on the Flow Characteristics and Mixing Performance of Multi-blade Combined Agitator. CIESC Journal, 2020, 71(11): 4964-4970.
[13]Wang Chunlin, LI Tingting, MA Qinyong. Numerical Simulation of the Slurry Consistence through the Impeller of the Slurry Pump. Journal of Drainage and Irrigation Machinery Engineering, 2007, 25(2): 16-18.
[14]QIAN Zhongdong, ZHANG Kai, WANG Zhiyuan. Effect of Blade Leading Edge Shape on Sediment Erosion of Blade in Double-suction Centrifugal Pumps. Journal of Drainage and Irrigation Machinery Engineering, 2014, 32(2): 103-107.
[15]WU Bo, YAN Hongzhi, DUAN Yiqun. Study on 3-D Turbulence Numerical Simulation and Wear Characteristics of Slurry Pump. China Mechanical Engineering, 2009, 20(6): 719-722.
[16]BAKKER S.A Computational modeling of materials. Minerals and Metals Processing: TMS, 2001.
[17]J.J D. Numerical simulation of solids suspension in a stirred tank. American

Institute of Chemical Engineer Journal, 2003, 49(11): 2700-2714.
[18]J.F A. Contact and Rubbing of Flat Surfaces. Journal of Applied Physics, 1953, 24(8): 981-985.
[19]CHEN Li, LIU Chao, ZHOU Jiren, Numerical Simulation of Flow in the Outlet Passages of Reversible Pumping Station by RNG k-ε Turbulent Model with Wall-function Law. Advances in Water Science, 2004, 15(1): 109-112.
[20]Archard J F Contact and Rubbing of Flat Surfaces. Journal of Applied Physics, 1953, 24(8): 981-98